# A Quadruple Mutant T4 RNA Hairpin with the Same Structure as the Wild-Type Translational Repressor†

Suman R. Mirmira and Ignacio Tinoco, Jr.*

*Department of Chemistry, University of California, and Structural Biology Division, Lawrence Berkeley National Laboratory, Berkeley, California 94720*

*Received February 21, 1996; Revised Manuscript Received April 8, 1996*⊗

ABSTRACT: The solution structure of a 16-nucleotide RNA hairpin, 5′-GCCUAG[CAAC]CUGGGC (loop bases in square brackets), has been determined by proton, phosphorus, and carbon (natural abundance) nuclear magnetic resonance (NMR) spectroscopy. This RNA tetraloop hairpin varies in four loop nucleotides from the wild-type T4 RNA hairpin (with eight loop nucleotides) involved in the translational repression of bacteriophage T4 DNA polymerase. Despite the differences in their sequence and proposed secondary structures, these two hairpins bind T4 DNA polymerase with equal affinity. The NMR spectra of the mutant hairpin indicate that its stem is extended in comparison to that of the wild-type hairpin by the formation of two additional Watson−Crick base pairs. The NMR data provide a precisely defined structure for the mutant hairpin with an average root mean square deviation of approximately 0.7 Å for all 16 residues in the molecule. The structure of the mutant loop is very similar to that determined previously for the wild-type hairpin. The three loop bases that are conserved between the mutant and wild-type hairpins point out in solution with the groups capable of hydrogen bond formation exposed to the solution. This is exactly what was seen for the wild-type hairpin. Also, unusual, long-range NOEs, loop hydrogen bonds, and even the position at which the loop bends are common features between the two loops. This explains how two different hairpins, by adopting similar three-dimensional structures, have the same affinity for the DNA polymerase.

In bacteriophage T4 the protein product of gene *43* (gp43) is a DNA polymerase that regulates its own synthesis by binding its mRNA at the ribosome-binding site and preventing translational initiation (Andrake et al., 1988). The minimum operator length required for DNA polymerase binding is a 36-nucleotide sequence that includes a hairpin containing a five-base-pair stem and an eight-nucleotide loop. This hairpin, referred to as the "wild-type" hairpin, was found to be crucial for polymerase binding (Tuerk et al., 1990). Mutations that disrupt the stem reduce the strength of the protein−RNA binding significantly. Also, randomization of the loop nucleotides results in a 50−60-fold decrease in polymerase binding, demonstrating a bias for this loop sequence.

In order to test whether any other loop sequence bound the polymerase with comparable affinity, selection experiments were done in which the loop nucleotides of the T4 hairpin were randomized and selected on the basis of affinity for polymerase (Tuerk & Gold, 1990). These experiments showed that two hairpins, the wild-type and a quadruple mutant (referred to as the "mutant hairpin"), bound the polymerase with equal affinity ($K_d$ = 4.8 nM). As shown in Figure 1, the two selected hairpin sequences have not only different sequences but also very different proposed secondary structures—the wild-type has a short stem and a loop of eight nucleotides, whereas the mutant has a long stem and a tetraloop. It is surprising that both these hairpins bind the polymerase with equal affinity. What kind of structure do they present to the polymerase? Are their three-dimensional solution structures similar despite their differing sequences and proposed secondary structures? Or, are there other interactions that allow the polymerase to bind two different hairpins with equal affinity? In order to answer these questions, we studied the three-dimensional structures of both hairpins using nuclear magnetic resonance (NMR)[1] spectroscopy.

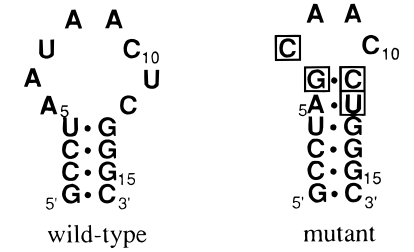


FIGURE 1: Sequence and proposed secondary structures of the wild-type and mutant hairpin. The positions at which the sequence of the two hairpins differ have been boxed.

The structure of the wild-type hairpin has been previously determined (Mirmira & Tinoco, preceding paper in this issue). In this paper, we present the results of our structural

† This research was supported in part by grants from the National Institutes of Health (GM 10840), the Department of Energy (DE-FG03-86ER60406), and by instrumentation grants from the Department of Energy (DE-FG05-86ER75281) and the National Science Foundation (DMB 86-09305 and BBS 87-20134).

* To whom correspondence should be addressed.

⊗ Abstract published in *Advance ACS Abstracts,* May 15, 1996.

[1] Abbreviations: UV, ultraviolet; EDTA, ethylenediaminetetraacetic acid; NMR, nuclear magnetic resonance; FID, free induction decay; 1D, one dimensional; 2D, two dimensional; ppm, parts per million; NOESY, nuclear Overhauser effect spectroscopy; COSY, correlation spectroscopy; HMQC, heteronuclear multiple-quantum correlation spectroscopy; TOCSY, total correlation spectroscopy; rMD, restrained molecular dynamics; RMSD, root mean square deviation; TSP, 3-(trimethylsilyl)-1-propanesulfonate; TMP, trimethyl phosphate.

S0006-2960(96)00415-1 CCC: $12.00 

studies on the mutant hairpin as well as a comparative study of the two structures. One-dimensional and two-dimensional, homonuclear and heteronuclear NMR experiments were used to assign the proton, carbon, and phosphorus resonances and to obtain the distance and torsion angle constraints used to calculate the structure. Restrained molecular dynamics calculations were used to calculate structures consistent with the NMR data.

## MATERIALS AND METHODS

*RNA Synthesis and Purification*. The RNA oligonucleotide 5′-GCCUAG[CAAC]CUGGGC-3′ was synthesized *in vitro* using T7 RNA polymerase from a synthetic single-stranded DNA template with a double-stranded promoter region (Milligan et al., 1987; Wyatt et al., 1991). Crude RNA was purified using denaturing 20% polyacrylamide gel electrophoresis. The yield of RNA was approximately 10 nmol of purified RNA/mL of reaction. Purified RNA was dialyzed extensively (>72 h) against a sodium phosphate and EDTA buffer and finally dissolved in 10 mM sodium phosphate and 10 $\mu$M EDTA, pH 6.0. For the various experiments on the mutant hairpin, the buffer, pH, and temperature (for NMR spectra) conditions were kept as close as possible to those used for the wild-type hairpin so as to be able to determine the structures of both hairpins under near-identical conditions.

*Thermodynamics.* Ultraviolet (UV) absorbance melting curves were obtained and analyzed to get thermodynamic parameters (Puglisi & Tinoco, 1989). The molecularity of the system was determined from UV absorbance melting curves obtained over an approximately 100-fold concentration range (7.7−782 $\mu$M) of the RNA sample. The experimental setup was identical to that used for the wild-type hairpin (see preceding paper).

*NMR Spectroscopy.* RNA samples used to measure NMR spectra were dissolved in 10 mM sodium phosphate and 10 $\mu$M EDTA, pH 6.0. Samples used to measure exchangeable spectra were lyophilized and then suspended in 400 $\mu$L of 90% $H_2O$/10% $D_2O$, while those used to measure nonexchangeable spectra were lyophilized several times from 99.96% $D_2O$ (Aldrich) and then suspended in 400 $\mu$L of 99.996% $D_2O$ (Cambridge Laboratories). The concentration of the RNA sample was approximately 2.5 mM. The samples were annealed at 65 °C for 2 min and cooled in ice for at least 5 min prior to each experiment. All proton and carbon chemical shifts were referenced to TSP. Most NMR spectra, with the exception of the $^1H-^{31}P$ HETCOR (heteronuclear correlation spectroscopy), were recorded on either a GE GN-500 or a BRUKER AMX-600 spectrometer. The $^1H-^{31}P$ HETCOR was recorded on a BRUKER AMX-300. All data processing was done with FELIX v. 2.3 (Biosym Technologies, Inc.).

The NMR experiments recorded for the mutant hairpin as well as the experimental parameters were very similar to those recorded for the wild-type hairpin (see preceding paper). One-dimensional (1D) exchangeable proton spectra, similar to those recorded for the wild-type hairpin, were recorded over a temperature range of 5 to 45 °C on the GN-500 using the 1-1 water suppression sequence (Plateau & Gueron, 1982). A 1D exchangeable proton spectrum of the mutant was also recorded at ≈2 °C on the AMX-600 using the same pulse sequence. A total of 4096 real points was collected over a spectral width of either 10 000 Hz (for the GN-500) or 12 500 Hz (for the AMX-600). 1D nonexchangeable spectra at different temperatures and $T_1$ measurements similar to those measured for the wild-type hairpin were also measured for the mutant.

The same repertoire of two-dimensional (2D) NMR experiments used for the wild-type molecule (see preceding paper) was used to assign as well as to obtain distance and torsion angle constraints for the mutant. Apart from minor differences in the number of scans or FIDs collected, the NMR spectra of the mutant hairpin were collected and processed in a manner identical to that of the wild-type hairpin.

In the case of the mutant hairpin, there was some spectral overlap at 25 °C. However, since the spectra used to get the distance and torsion angle constraints for the wild-type hairpin were recorded at 25 °C, we continued to use spectra recorded at 25 °C for the mutant hairpin as well. Some 2D spectra were recorded at 15 °C to resolve the overlapped peaks and to help with the assignment of the different resonances. All distance and torsion angle constraints were obtained from spectra recorded at 25 °C.

*Interproton Distances and Scalar Coupling Measurements.* Interproton distances between nonexchangeable protons were derived from NOESY peak intensities at different mixing times (50, 100, 150, and 400 ms). The intensities of the cross peaks in the different NOESY experiments were used to classify the peaks into four categories: strong (1.8−3.0 Å), medium (2.0−4.0 Å), weak (2.5−5.0 Å), and very weak (3.0−7.0 Å). The most intense peaks in the 50 ms NOESY were assigned the distance range 1.8−3.0 Å, and peaks with weaker intensities were assigned the range 2.0−4.0 Å. Peaks that were not seen in the 50 ms NOESY, but appeared in the 100 ms NOESY, and were clearly present in the 150 ms NOESY were assigned the range 2.5−5.0 Å. Peaks that were not present in either the 50-, 100-, or 150 ms NOESY spectra but were present in the 400 ms NOESY were assigned the distance range 3.0−7.0 Å. Exchangeable proton−proton NOEs were given looser constraints—the imino to imino cross peaks between base pairs were assigned a distance range of 3.0−5.0 Å. A total of 266 interproton distance constraints was obtained from the NMR spectra of this RNA molecule.

The scalar couplings were measured and the torsion angle constraints were determined in the same way as for the wild-type hairpin (see preceding paper). The calculation of the structure also followed the same protocol (generation of 20 random starting structures which were then subjected to global folding, refinement protocol, and a final minimization step) as used for the wild-type hairpin.

*Comparison of Wild-Type and Mutant Hairpin Structures.* The molecular dynamics program X-PLOR (Brünger, 1990) was used to generate three-dimensional structures of both hairpins, consistent with the constraints derived from their NMR data. For each hairpin, 20 starting structures with randomized torsion angles were generated within X-PLOR and then subjected to the global fold (see preceding paper for details of structure calculation). Converged structures were then subjected to the refinement protocol and the final minimization step. The final structures for each hairpin were superimposed and an average structure was obtained. The average structure of one hairpin was then superimposed onto the average structure of the other on the basis of the three

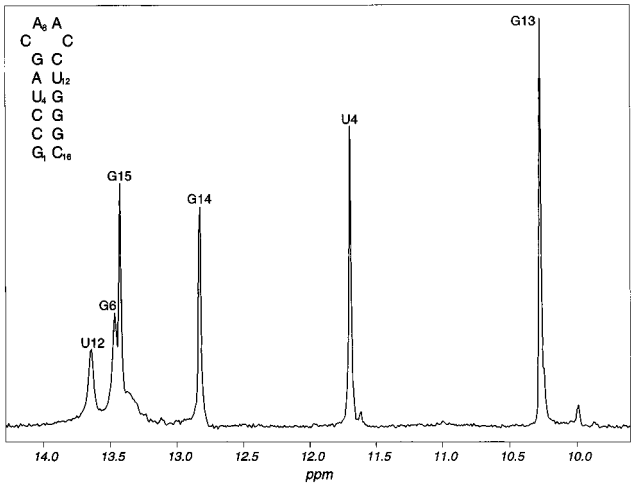


FIGURE 2: One-dimensional imino spectrum of the 16-nucleotide mutant RNA hairpin in 90% $H_2O$/10% $D_2O$ recorded at 2 °C on a GN-500 spectrometer using the 1-1 water suppression pulse sequence.

conserved loop nucleotides to obtain the RMSD with which the two hairpin loops superimpose. The structures of the entire loop could not be superimposed as the sequence is not the same and X-PLOR requires identical atoms in order to superimpose any two given structures.

## RESULTS

### *Structure of Mutant Hairpin*

*Thermodynamics.* UV absorbance melting curves of the mutant RNA hairpin showed no change (within experimental error) in the melting temperature ($T_m$) over a 100-fold concentration range, as expected for a unimolecular system. Fitting the melting curve data to a two-state, unimolecular model yielded $\Delta H° = -43 \pm 2$ kcal/mol, $\Delta S° = -129 \pm 4$ cal/(K mol), and $T_m = 58 \pm 1$ °C.

*NMR Analysis. (A) Assignment and Analysis of the Exchangeable Proton Spectra.* The 1D imino spectrum of the 16-nucleotide mutant RNA hairpin is shown in Figure 2. Four sharp imino resonances similar to the ones seen for the wild-type hairpin are seen in the spectrum. These resonances belong to the imino protons of $U_4$ (11.68 ppm) and $G_{13}$ (10.26 ppm) of the G·U pair and to $G_{14}$ (12.81 ppm) and $G_{15}$ (13.41 ppm). Two extra peaks and a shoulder are seen at 13.45 ppm ($G_6$), 13.62 ppm ($U_{12}$), and 13.37 ppm ($G_1$), respectively. Assignments of the imino protons were confirmed from a 2D nuclear Overhauser effect spectroscopy (NOESY) experiment of the hairpin in 90% $H_2O$/10% $D_2O$ recorded at 2 °C. A strong NOE was seen between the imino protons of $U_4$ and $G_{13}$. Weaker imino−imino cross peaks, which indicate stacking of the base pairs to form helical stems, were seen between $U_4$ and $G_{14}$, $G_{13}$ and $G_{14}$, and $G_{14}$ and $G_{15}$. In the NOESY spectrum, the $G_6$ imino peak was broadened and partially overlapped with that of $G_{15}$'s. However, its assignment was confirmed on the basis of the cross peaks seen to the aminos and H5 of $C_{11}$. The $U_{12}$ imino peak was not seen in the NOESY experiment, but its assignment was confirmed by the cross peak seen at the $A_5$-H2 frequency. We believe that the missing $U_{12}$ and broadened $G_6$ iminos seen in the NOESY spectrum as well as the weakened intensity of these peaks in the 1D imino spectrum result from exchange with the solvent. This is consistent with 1D imino spectra recorded at different temperatures which showed that after the $G_1$ imino resonance, the imino resonances of $G_6$ and $U_{12}$ are the next to broaden and disappear; it is consistent with a stem that frays apart at its ends. As seen for the wild-type hairpin (see preceding paper), as the temperature is increased, the peaks corresponding to the imino protons of the guanine and uracil involved in the G·U pair were the last to broaden or disappear. Assignments of the aminos in the stem were made from the same exchangeable NOESY experiment using the assignment pathways typically seen in an A-form stem (Heus & Pardi, 1991).

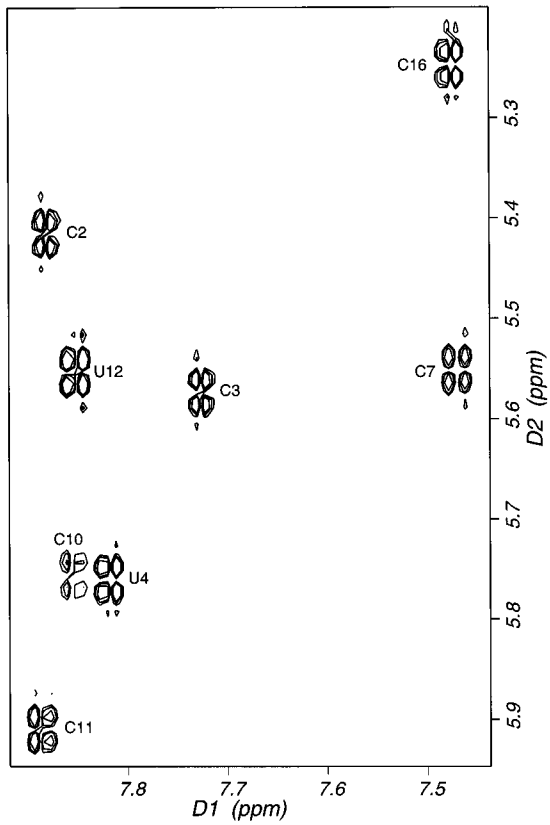


FIGURE 3: H6 (horizontal axis) to H5 (vertical axis) region of a DQF-COSY spectrum for the mutant hairpin in $D_2O$ recorded at 25 °C on a GN-500 spectrometer. Only eight peaks are seen. This is consistent with a single conformation for the hairpin with eight pyrimidines.

*(B) Assignment and Analysis of the Nonexchangeable Proton Spectra.* Assignment of the nonexchangeable protons is one of the most important steps in obtaining a high-resolution structure of a molecule. The more complete the assignments, the greater the number of both distance and torsion angle constraints that one can obtain. For the mutant hairpin we were able to assign all the H8s, H6s, H2s, H5s, H1′s, and H2′s, all but one of the H3′s and H4′s, and 22 of the 32 H5′s/H5″s in the molecule. We were also able to assign 13 of the 15 $^{31}P$ resonances. This near-complete assignment of the mutant hairpin provided a large number of constraints for the determination of its structure. We followed standard methods (Varani & Tinoco, 1991) for the assignment of the nonexchangeable protons in the spectra.

Figure 3 shows the H5−H6 region of a DQF-COSY spectrum of the mutant hairpin acquired in $D_2O$. The number of H5−H6 cross peaks observed in the spectrum is consistent with a single conformation of the hairpin which contains

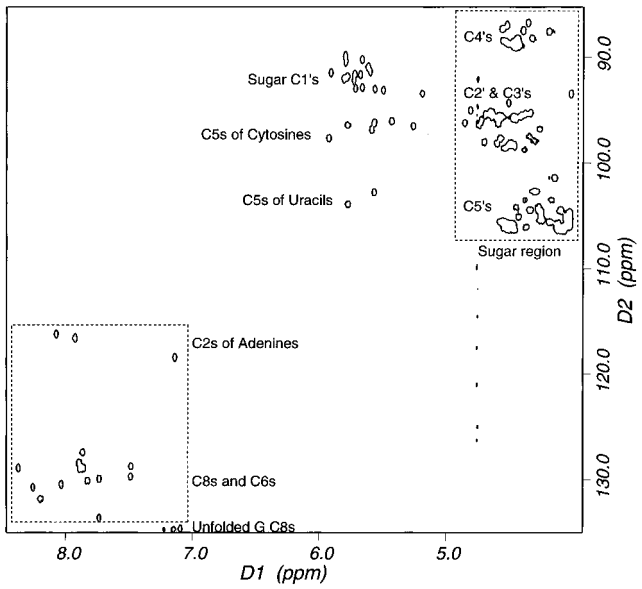


FIGURE 4: Natural abundance $^1H-^{13}C$ HMQC spectrum of the hairpin in $D_2O$. This spectrum was recorded at 25 °C on an AMX-600 spectrometer. The $^1H$ dimension is on the horizontal axis, and the $^{13}C$ dimension is on the vertical axis. The C2′, C3′, C4′, and C5′ resonances as well as the aromatic (C6, C8, and C2) resonances were folded in. Only the uracil and cytosine C5s, the sugar C1′s, and three of the guanine C8 resonances were not folded. The boxes drawn with dotted lines enclose the resonances that have folded in. The C8s and C6s resonate at ≈140 ppm, the C2s resonate at ≈153 ppm, and the sugar carbons (except C1′) resonate from ≈63 to ≈83 ppm.

eight pyrimidines. A natural abundance $^1H-^{13}C$ HMQC spectrum (Figure 4) helped distinguish the uracil H5 resonances from the cytosine H5 resonances on the basis of the difference in the chemical shifts of their C5 resonances.

The adenine H2 peaks were distinguished from the purine H8 peaks on the basis of their longer $T_1$ relaxation times as well as on the basis of the chemical shifts of their directly bonded carbon atoms (C2s) using the natural abundance $^1H-^{13}C$ HMQC spectrum shown in Figure 4. The information from this spectrum and the DQF-COSY as well as from a NOESY and $^1H-^{13}C$ HMQC recorded at 15 °C helped in the aromatic to anomeric proton assignment of the mutant hairpin. Chemical shifts of the protons belonging to nucleotides $G_1$ to $U_4$ and $G_{13}$ to $C_{16}$ were similar to those for the corresponding protons in the wild-type hairpin. This was an added help in the assignment process.

Figure 5 shows the H8/H6/H2−H5/H1′ region of a 400 ms NOESY spectrum. The H8/H6−H1′ connectivities were continuous from $G_1$ to $C_{16}$, although standard A-form connectivities were seen only from $G_1$ to $G_6$ and from $C_{11}$ to $C_{16}$. Characteristically A-like sequential and cross-strand NOEs are seen from the H2 of $A_5$ to the H1′s of $G_6$ and $G_{13}$. This spectrum also shows the presence of an unusual and long-range NOE from $A_9$H8 to $C_7$H1′. This peak, which was seen in both the 150 ms and 400 ms NOESY spectra, is similar to what was seen in the case of the wild-type hairpin.

The H2′ resonances were mostly assigned from the H1′−H2′ region of a 100 ms NOESY. Independent assignment pathways using the H8/H6−H2′ connectivities thus established showed that the H8/H6−H2′ connectivities were continuous from $G_1$ to $C_{16}$. Standard A-like connectivities were seen from $G_1$ to $G_6$ and from $C_{11}$ to $C_{16}$. In most cases, the H2′($i$)−H1′($i$+1) and H2′($i$)−H5($i$+1) connectivities provided further corroboration for the assignments.

Correlated spectra were the most important means of assignment for the remainder of the sugar protons. A high-resolution, $^{31}P$-decoupled DQF-COSY, which enabled observation of resonances separated by as little as 0.04 ppm, was used to assign the different sugar spin systems on the basis of the characteristic multiplet structures of the H2′−H3′, H3′−H4′, H4′−H5′/5″, and H5′−H5″ cross peaks (Varani & Tinoco, 1991). A TOCSY spectrum which showed cross peaks from the H1′ proton to the H2′, H3′, and H4′ protons of some loop nucleotides (which had $J_{1'2'} > 2$ Hz) confirmed the assignments obtained from the DQF-COSY. The assignments of the sugar resonances were also confirmed from the intranucleotide NOEs observed from the H8/H6 proton to the sugar protons in a 400 ms NOESY spectrum. Independent assignment pathways using the H8/H6−H3′ connectivities was also established.

Sequence-specific carbon assignments for the base and C1′ resonances were obtained from the natural abundance $^1H-^{13}C$ HMQC spectrum shown in Figure 4 using the available proton assignments. The 3 adenine C2 resonances and 13 of the 16 aromatic resonances were folded about the 135 ppm frequency. However, three of the aromatic resonances (corresponding to the C8s of $G_6$, $G_{14}$, and $G_{15}$) resonate at ≈134.7 ppm and are not folded over. Two of these resonances, the C8s of $G_{14}$ and $G_{15}$, were not seen in the HMQC spectrum of the wild-type hairpin (see preceding paper). We believe that they must have been shifted slightly more downfield, closer to 135 ppm, and were hence nulled when the spectrum folded about the 135 ppm frequency. The appearance of the three peaks upfield of 135 ppm indicates that this is not an unusual chemical shift for the C8s of guanine residues in a base-paired stem. It also emphasizes the need for careful planning when folding a spectrum. Had the wild-type spectrum been folded about a different frequency, these peaks would have been seen. However, since our interest in this region of the spectrum was to distinguish between the adenine H2−C2 peaks and the purine H8−C8 peaks, and since that purpose was met, we did not redo these experiments.

The $^1H-^{31}P$ HETCOR, which provides information about the sugar sequence along the backbone, was assigned using the previously determined H3′ and H5′/H5″ assignments. A strong sequential H3′($i$)−$^{31}$P($i$+1) cross peak and weak intranucleotide H5′/H5″−$^{31}$P cross peaks were seen at the $^{31}P$ resonances. These scalar connectivities unambiguously confirmed the nucleotide sequence, especially in the loop region where structural assumptions cannot be made.

The proton, carbon, and phosphorus assignments are summarized in Table 1.

*Distance and Torsion Angle Constraints.* Distance constraints were obtained from NOESY spectra at different mixing times as described in the Materials and Methods section. A total of 266 interproton distance constraints were obtained from the NOESY spectra. An additional four constraints for each of the C·G and A·U pairs and five constraints for the $U_4$·$G_{13}$ pair were used to maintain the hydrogen bonding between the paired bases and to keep them planar.

Unusual, long-range NOEs played a very important role in the calculation of the structure. Such NOEs were seen in the 150 and 400 ms NOESY experiments from $A_9$H8 to the H1′ and H2′ resonances of $C_7$. These NOEs are very similar to those seen in the wild-type hairpin (see preceding paper).

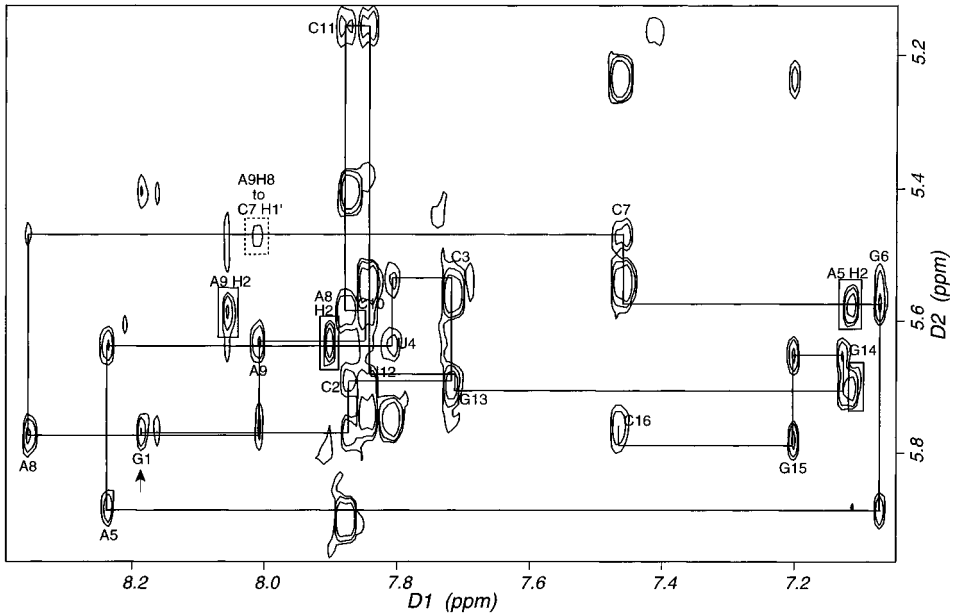


FIGURE 5: Aromatic to anomeric region of a 400-ms NOESY acquired at 25 °C on an AMX-600 spectrometer. The H8/H6($i$)−H1′($i$)−H8/H6($i$+1) walk is shown in solid lines. The nucleotides have been labeled near the cross peak that corresponds to the intranucleotide H8/H6−H1′ NOEs. The large, unlabeled peaks seen along the pyrimidine H6 resonances are the intranucleotide H5−H6 cross peaks. The arrow indicates the start of the walk at the $G_1$H8−$G_1$H1′ cross peak. The cross peak corresponding to the unusual, long-range connectivity ($A_9$H8 to $C_7$H1′) is enclosed in a dotted box. The AH2−H1′ (both sequential and cross strand) have been boxed by solid lines.

The torsion angle constraints were obtained largely from the correlated spectra although some information was available from the NOESY spectra. All H8/H6−H1′ NOEs were weak, indicating that the conformation about the glycosidic angle is anti for all nucleotides. $\chi$ was restricted to a range of $-160° \pm 50°$ for all the residues in the molecule.

The backbone conformation is determined by six torsion angles for each nucleotide (Saenger, 1984). These torsion angles were estimated on the basis of the scalar couplings of the sugar protons with each other and with $^{31}$P as well as on the $^{31}$P chemical shifts. The measured scalar couplings are reported in Table 2.

The torsion angles adjacent to the phosphorus atom, i.e., α (O3′−P) and ζ (P−O5′), were estimated from the chemical shifts of the $^{31}$P resonances (Gorenstein, 1984). The chemical shifts of the stem $^{31}$P's lie within approximately 0.5 ppm. For these nucleotides, both α and ζ were assigned to gauche conformations. No assumptions were made about the phosphorus resonances that were shifted downfield ($G_6pC_7$, $C_7pA_8$, or $C_{10}pC_{11}$) as several conformational effects could be responsible for this shift (Giessner-Prettre et al., 1984). The phosphorus of $C_{10}$ ($A_9pC_{10}$) is shifted upfield from the stem $^{31}$P resonances. This has been seen before for $^{31}$P resonances from single-stranded regions or regions close to the junction between single- and double-stranded regions (Williamson & Boxer, 1989; Varani et al., 1991). Taking a conservative approach, no constraints were used for either the α or the ζ torsion angles for any of the loop nucleotides ($G_6pC_7$, $C_7pA_8$, $A_8pA_9$, $A_9pC_{10}$, or $C_{10}pC_{11}$).

The conformations around $\beta$, $\gamma$, and $\epsilon$ were obtained from scalar couplings. Torsion angles $\beta$ and $\epsilon$ were estimated from the heteronuclear $^1$H−$^{31}$P couplings (H5′−P and H5″−P for $\beta$ and H3′−P for $\epsilon$) obtained from the $^1$H−$^{31}$P HETCOR experiment. $\gamma$ was estimated from the H4′−H5′ and H4′−H5″ couplings obtained from the high-resolution DQF-COSY experiment. Scalar couplings, both homonuclear and heteronuclear, involving H5′ and H5″ were obtained without stereospecific assignments.

For the stem nucleotides, $\beta$ was constrained to be trans ($180° \pm 20°$), as expected in standard A-form RNA. All four loop residues ($C_7$, $A_8$, $A_9$, and $C_{10}$) showed very small H5′−P and H5″−P couplings (Table 2) as expected for a trans $\beta$. $\beta$ was constrained to be trans for these residues as well; however, a much broader range ($\pm 40°$) was used.

$\gamma$ was restricted to the standard A-form range of gauche$^+$ for most of the nucleotides. Tight constraints ($55° \pm 20°$) were used for the stem residues $C_2$, $C_3$, $U_4$, $G_{13}$, $G_{14}$, $G_{15}$, and $C_{16}$. A broader range ($55° \pm 30°$) was used for the nucleotides nearer the stem−loop junction ($A_5$, $G_6$, $C_7$, $C_{10}$, $C_{11}$, and $U_{12}$) as well as for $G_1$. Both adenine residues in the loop ($A_8$ and $A_9$) showed H4′−H5′ and H4′−H5″ couplings >3 Hz, indicating that $\gamma$ is in equilibrium between the different conformations and hence $\gamma$ was not constrained for these nucleotides.

The angle $\epsilon$ is characterized by the H3′−P coupling. Although it is known that the gauche$^+$ form is never populated due to steric hindrances, the other two conformers, gauche$^-$ and trans, are both allowed and cannot be distinguished on the basis of the H3′−P coupling alone (Altona, 1982). This torsion angle was constrained to the standard A-form value of $-155° \pm 20°$ (Saenger, 1984) for most residues in the stem ($G_1$ to $A_5$ and $G_{13}$ to $G_{15}$). A broader range ($-155° \pm 40°$) was used for some nucleotides ($G_6$, $C_{11}$, and $U_{12}$) near the stem−loop junction. This torsion angle was not used for any of the loop nucleotides.

Nucleotides were constrained to be either C3′-*endo* or intermediate between C3′-*endo* and C2′-*endo* by constraining the four endocyclic torsion angles in the sugar ring ($\nu_0$, $\nu_1$, $\nu_2$, and $\nu_3$). Very few weak cross peaks were seen in the H1′−H2′ region of the DQF-COSY, indicating predominantly C3′-*endo* sugar pucker for all the nucleotides. The few cross peaks seen in this region of the COSY spectrum correspond to the residues in the loop. The magnitude of their H1′−H2′ couplings is small, indicating that while the sugar pucker is in equilibrium between C3′-*endo* and C2′-*endo*, the equilibrium is favored toward the C3′-*endo*

Table 1: Proton, Carbon, and Phosphorus Chemical Shifts (ppm) for the Mutant RNA Hairpin in 10 mM Sodium Phosphate and 10 $\mu$M EDTA, pH 6.0[a]

| residue | H8/H6 | H2/H5 | H1′ | H2′ | H3′ | H4′ | H5′/5″ [b] |
|---|---|---|---|---|---|---|---|
| G1 | 8.19 | na | 5.77 | 4.84 | 4.73 | 4.55 | 4.44/4.26 |
| C2 | 7.87 | 5.41 | 5.69 | 4.55 | 4.51 | 4.25 | |
| C3 | 7.72 | 5.56 | 5.54 | 4.63 | 4.37 | 4.45 | (4.11) |
| U4 | 7.81 | 5.75 | 5.64 | 4.32 | 4.59 | 4.44 | (4.49/4.09) |
| A5 | 8.24 | 7.11 | 5.89 | 4.67 | 4.69 | 4.47 | 4.56/4.17 |
| G6 | 7.07 | na | 5.58 | 4.36 | 4.29 | 4.42 | 4.16/4.04 |
| C7 | 7.46 | 5.54 | 5.47 | 4.40 | 4.48 | 4.31 | 4.36/4.06 |
| A8 | 8.36 | 7.90 | 5.77 | 4.80 | 4.58 | 4.34 | 4.23/4.01 |
| A9 | 8.01 | 8.06 | 5.63 | 4.49 | 4.63 | 4.51 | 4.25/4.01 |
| C10 | 7.85 | 5.75 | 5.59 | 4.46 | 4.58 | 4.38 | 4.33/4.09 |
| C11 | 7.88 | 5.90 | 5.15 | 4.43 | 4.25 | (4.29) | |
| U12 | 7.84 | 5.54 | 5.70 | 4.64 | 4.56 | 4.44 | |
| G13 | 7.72 | na | 5.70 | 4.71 | 4.33 | 4.54 | 4.36/4.16 |
| G14 | 7.13 | na | 5.65 | 4.57 | 4.53 | 4.43 | |
| G15 | 7.20 | na | 5.78 | 4.44 | | | (4.01) |
| C16 | 7.47 | 5.24 | 5.76 | 4.00 | 4.13 | 4.18 | 4.47/4.02 |

| residue | imino | amino | C8/C6 | C2/C5 | C1′ | P |
|---|---|---|---|---|---|---|
| G1 | 13.37 | | 138.2 | na | 90.5 | na |
| C2 | na | 8.81/7.08 | 141.0 | 96.1 | 93.0 | −4.11 |
| C3 | na | 8.40/7.02 | 140.0 | 96.9 | 93.0 | −4.05 |
| U4 | 11.68 | na | 139.9 | 103.9 | 90.2 | |
| A5 | na | 7.70/6.44 | 139.2 | 151.5 | 91.5 | −4.46 |
| G6 | 13.45 | | 134.7 | na | 91.4 | −3.95 |
| C7 | na | | 141.2 | 96.2 | 93.1 | −2.99 |
| A8 | na | | 141.1 | 153.4 | 89.9 | −2.74 |
| A9 | na | | 139.5 | 153.8 | 92.9 | −3.49 |
| C10 | na | 8.40/7.44 | 142.6 | 96.4 | 90.9 | −4.73 |
| C11 | na | 8.61/7.20 | 141.6 | 97.7 | 93.5 | −2.98 |
| U12 | 13.62 | na | 141.1 | 102.8 | 91.6 | −4.25 |
| G13 | 10.26 | 8.26/6.10 | 136.3 | na | 92.2 | −3.71 |
| G14 | 12.81 | 8.64/6.40 | 134.7 | na | 91.7 | |
| G15 | 13.41 | 7.88/7.08 | 134.8 | na | 92.0 | −3.96 |
| C16 | na | 8.44/7.21 | 140.2 | 96.5 | 91.9 | −4.27 |

[a] All proton and carbon shifts were referenced to TSP, and phosphorus chemical shifts were referenced to TMP. Imino and amino resonances were measured at 2 °C. All other proton, carbon, and phosphorus resonances were measured at 25 °C. Values in parentheses are tentative. na = not applicable. [b] For the assignment of the H5′ and H5″ resonances, the assumption made was that the H5′ proton resonates downfield from the H5″.

Table 2: Scalar Couplings (in Hz) for the Mutant Hairpin at 25 °C in 10 mM Sodium Phosphate and10 $\mu$M EDTA, pH 6.0[a]

| residue | $J_{1'2'}$ | %N | $J_{2'3'}$ | $J_{3'4'}$ | $J_{4'5'/5''}$ | $J_{5'5''}$ | $J_{P(i+1)3'}$[b] | $J_{P(i)5'/5''}$[b] |
|---|---|---|---|---|---|---|---|---|
| G1 | 2.5 | 80 | 4.5 | 7.7 | <2/4.3 | 11.7 | 8.0 | |
| C2 | <2 | >90 | 3.7 | | | | | |
| C3 | <2 | >90 | 4.0 | 9.9 | | | | |
| U4 | 2.2 | 85 | 4.2 | 9.5 | | | 6.3 | |
| A5 | <2 | >90 | 4.6 | 9.2 | <2/4.3 | 10.3 | 9.0 | <2/2.9 |
| G6 | 2.2 | 85 | 4.3 | 9.4 | | | ≈6 | |
| C7 | 2.4 | 83 | 5.0 | 9.0 | <2/4.4 | 10.3 | 9.1 | |
| A8 | 3.2 | 70 | 4.2[b] | 6.6 | 4.2/3.7 | 12.2 | 8.6 | <2/3.8 |
| A9 | 3.2 | 70 | 4.9 | 6.9 | ≈3[b]/4.0 | 11.8 | 7.1 | ≈3/2.7 |
| C10 | 3.6 | 64 | 4.3[b] | 7.2 | <2/4.1 | 11.3[b] | 8.4 | ≈3/<2 |
| C11 | >2 | >90 | 4.5 | 9.5 | | | 7.4 | |
| U12 | 2.2 | 84 | 4.0 | 8.8 | | | 6.7 | |
| G13 | <2 | >90 | 4.3 | 9.9 | <2/≈3[b] | | | ≈3/≈3 |
| G14 | 2.1 | 87 | 3.8 | 9.3 | | | 7.8 | |
| G15 | <2 | >90 | | | | | | |
| C16 | 2.1 | 87 | 4.4 | 8.7 | <2/≈3[b] | 10.9 | | |

[a] All uncertainties are ±0.5 Hz unless otherwise mentioned. For the H4′−H5′/H5″ and the P($i$)−H5′/H5″ couplings, the couplings to the downfield proton are reported first. [b] Uncertainties are ±1 Hz. When an approximate number is given, it is beacuse the peak was in a crowded region and a precise value of the coupling could not be measured.

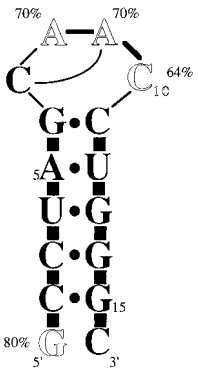


FIGURE 6: Schematic summary of the NMR data in this study. Nucleotides shown in solid type have C3′-*endo* sugar puckers while those in outline type are in equilibrium between C3′-*endo* and C2′-*endo* conformations. The percent (±7%) C3′-*endo* is shown next to the base. The solid line shows the nucleotides between which unusual, long-range NOEs are seen. The dots represent hydrogen-bonded imino protons. The black boxes between the bases indicate standard A-form stacking. In the loop region, the presence of connectivities from one residue to the next is shown by lines between the residues. The thick lines between $A_8$, $A_9$, and $C_{10}$ represent the stacking seen between them.

conformation. Most nucleotides were constrained to be C3′-*endo*. For those nucleotides for which weak H1′−H2′ cross peaks were seen, the four endocyclic torsion angles were constrained in a broad range which encompassed C2′-*endo*, C3′-*endo*, and the O4′-*endo* sugar conformations. The percent C3′-*endo* conformation (=% N) reported in Table 2 was calculated from the magnitude of the H1′−H2′ couplings (de Leeuw & Altona, 1982).

Figure 6 summarizes the data obtained from the different NMR experiments.

*Structure Calculations.* Using the distance and torsion angles determined as above, as well as empirical energy terms for bond lengths, bond angles, improper angles and van der Waals potential, we calculated three-dimensional structures of the mutant hairpin that were consistent with the NMR data. The entire 16-nucleotide sequence of the mutant RNA hairpin was used to generate 20 starting structures with randomized backbone torsion angles. These random structures were then subjected to the global fold protocol, followed by the refinement protocol and finally the energy minimization step as described in the preceding paper. Eighteen of the 20 converged to low-energy structures. None of these 18 final structures violate any of the experimentally derived NOE constraints by more than 0.2 Å, although there are minor violations of the distances used to constrain the hydrogen bonding between the base pairs.

In order to assess how precisely the structures were determined by the NMR data, these 18 structures were superimposed, and an average structure was calculated. The root mean square deviation (RMSD) for each structure compared to the average structure was then calculated. The average RMSD when all 16 nucleotides are superimposed is 0.72 Å (standard deviation = 0.31 Å) for the 18 converged structures. Figure 7a shows a ribbon representation of the phosphate backbones of all 18 converged structures of the mutant hairpin superimposed from residue $C_2$ to $G_{15}$. Figure 7b shows the overlap of the heavy atoms (all atoms excluding the hydrogen atoms) of these 18 structures superimposed from residue $C_2$ to $G_{15}$. The precision with which the structure has been determined can be seen in this figure.

It can be seen from Figure 7b that the six base pairs in the stem are not as precisely defined as the four nucleotides

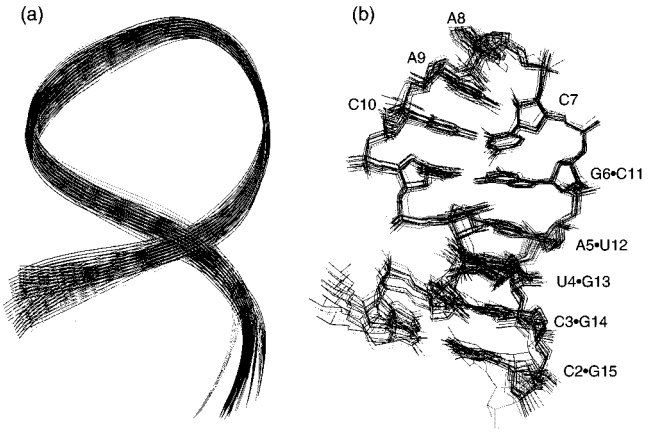


FIGURE 7: (a) Ribbon representation of the phosphate backbones of all 18 converged structures of the mutant hairpin superimposed from residue $C_2$ to $G_{15}$. (b) Overlap of the heavy atoms for all 18 structures of the mutant hairpin with the nucleotides numbered.

in the loop. Superimposing the six base pairs (nucleotides $G_1$ to $G_6$ and $C_{11}$ to $C_{16}$) of all 18 structures gave an average RMSD value of 0.69 Å (±0.35 Å) whereas the average RMSD for the loop nucleotides ($C_7$ to $C_{10}$) was 0.27 Å (±0.15 Å). We attribute the precision with which the loop nucleotides superimpose to the large number of NOE constraints used in the loop. Very few torsion angle constraints were used to constrain the loop. Torsion angles $\alpha$, $\zeta$, and $\epsilon$ were not constrained for any of the loop nucleotides, $\gamma$ was constrained for two of the four loop residues, and although $\beta$ was constrained for all four nucleotides, the range used was double that of the stem (±40° as opposed to ±20°). However, many more NOE (distance) constraints were available for the loop nucleotides, and this improved the precision. An average of 21 constraints were obtained per loop residue (a total of 84) as opposed to 15.2 per stem residue (a total of 182). The range of conformations that the loop could adopt is restricted by the requirement that the structure satisfy the many distance constraints that were obtained directly from the NMR data.

It is likely that this loop is stabilized by the formation of a hydrogen bond between the O2 of residue $C_7$ and the amino proton of $C_{10}$. Not only are they in the right geometry for hydrogen bond formation in all 18 structures, but the average distance between $C_7$O2 and $C_{10}$N4 is 2.6 ± 0.1 Å over all the structures. The average angle formed between the two heteroatoms is 150° (±4°). Also (as can be seen from Table 1), one of the amino protons of $C_{10}$ is shifted considerably downfield (8.40 ppm). This is indicative of its involvement in hydrogen bond formation. Taking a conservative approach, although the downfield-shifted amino proton was noticed, no constraints were used to form any hydrogen bond with the $C_{10}$ amino. As in the case of the wild-type hairpin, the bases of loop residues $A_8$, $A_9$, and $C_{10}$ are stacked on one another with their Watson−Crick faces pointing out into the solution in all the structures.

Figure 8 shows the three-dimensional structure of one of the final structures of the mutant hairpin. In this figure the proximity as well as the correct orientation for hydrogen bond formation between $C_7$O2 and the $C_{10}$ amino proton is visible.

All 18 structures were calculated with and without the electrostatics term in the force field and the results obtained in both cases were similar. The electrostatics term appears to have had little or no impact on the structure of the loop.

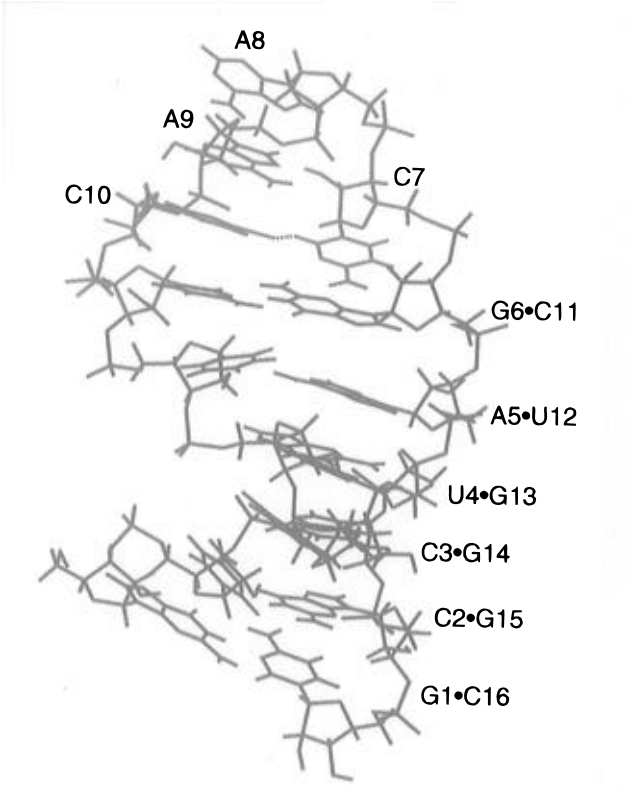


FIGURE 8: Representative structure of the mutant RNA hairpin. The hydrogen bond in the loop (between $C_7$O2 and the amino proton of $C_{10}$) is shown by black dashed lines.

The average RMSD values obtained for the superimposing of the loop nucleotides are very similar for the structures determined with and without the electrostatics term in the final minimization step.

*Comparison of Wild-Type and Mutant Hairpin Structures*

1D and 2D (NOESY) spectra of the samples in 90% $H_2O$/10% $D_2O$ were recorded for both hairpins. From the imino region of these spectra, it was apparent that while the wild-type hairpin had loop nucleotides stacked in A-form conformation over its short stem, the mutant actually had a base-paired stem that extended right up to $G_6$ and $C_{11}$. Correspondingly, it had a higher melting temperature (58 °C as opposed to the wild-type's 48 °C). These results are in agreement with its predicted secondary structure. However, the differences between the two hairpins more or less ends with this.

Even before the final structure of the mutant was calculated, the first similarity between the two hairpins that we noticed (and one which also simplified the assignment of the resonances for the mutant hairpin) was that the chemical shifts of some of the stem nucleotides were similar. While one would expect that the first three pairs would show similarities in the chemical shifts of their protons, that most of the protons of $U_4$ and $G_{13}$ had identical (within 0.02 ppm) chemical shifts was surprising. This indicates that despite the differences in sequence, the chemical environment around this pair is very similar in the two hairpins. In the wild-type hairpin, the stem is extended by A-form stacking of three nucleotides on the 5′ side and one nucleotide on the 3′ side. This effectively leaves only four nucleotides ($A_8$, $A_9$, $C_{10}$, and $U_{11}$) in the loop. In the case of the mutant, the stem is extended by hydrogen-bonded base pair formation of two base pairs; once again leaving only four nucleotides

in the loop ($C_7$, $A_8$, $A_9$, and $C_{10}$). The two hairpins have effectively the same stem length and loop size.

The unusual and long-range NOEs seen in the loop of the wild-type hairpin were also seen in the case of the mutant hairpin. In the wild-type molecule, we see long-range NOEs from the aromatic proton of $A_9$ ($A_9$H8) to $U_7$H1′, $U_7$H2′, and $U_{11}$H1′. In the case of the mutant, we see similar NOEs from $A_9$H8 to $C_7$H1′ and $C_7$H2′. No long-range NOEs are seen to $C_{11}$ since it is base paired with $G_6$ and hence is no longer angled toward the loop.

The sequential H8/H6−H1′ as well as the H8/H6−H2′ and H8/H6−H3′ connectivities in the 400 ms NOESY were continuous for both molecules (except for overlapped and unassigned resonances where one cannot be sure). This indicates that there is no sharp bend or turn in either molecule and that the four loop nucleotides can comfortably span the gap between the two strands. No C2′-*endo* sugar puckers were seen for either molecule, although the loop nucleotides of both molecules were in equilibrium between C3′-*endo* and C2′-*endo* sugar pucker.

When the final structure was calculated, we found that the in-space orientation of the three conserved loop nucleotides ($A_8$, $A_9$, and $C_{10}$) was identical in both molecules. In both molecules we see that the bases of these loop residues are stacked on one another with their Watson−Crick faces pointing out into the solution. The constraints used for the loop residues were different in the two cases. All the constraints were based solely on the NMR data. While we did get a large number of distance constraints for the loops, the individual constraints themselves differed between the two molecules. Also, the torsion angle constraints used in the case of the wild-type were different from those used for the mutant. Weak or nonexistent intranucleotide H5′/H5″−$^{31}$P cross peaks allowed us to constrain the $\beta$ torsion angle for all the nucleotides (loop nucleotides were given a broader range) in the mutant hairpin, whereas in the case of the wild-type hairpin, only four of the eight loop nucleotides could be constrained, even with the broader range. Similarly, we were able to constrain $\gamma$, albeit loosely, for two of the four loop nucleotides in the mutant but none in the case of the wild type. Conversely, given the smaller range of $^{31}$P chemical shifts in the wild-type hairpin, the $\alpha$ and $\zeta$ torsion angles for some loop residues were constrained to be gauche, whereas no constraints were used for either $\alpha$ or $\zeta$ in the mutant hairpin right from the $G_6pC_7$ step to the $C_{11}pU_{12}$ step. Despite the different constraints, the two loops are remarkably alike; they even have an identical hydrogen bond—that between $C_7$O2 (mutant)/$U_7$O2 (wild type) and the $C_{10}$ amino proton. The geometry as well as the distance between these atoms is perfect for hydrogen bond formation in all the structures of both molecules. This hydrogen bond is further evidenced by the downfield-shifted $C_{10}$ amino proton in both hairpins. Despite a nucleotide substitution, this hydrogen bond is seen in both hairpins.

The final test to see exactly how similar these two hairpin loops are was to superimpose them one onto the other. An average structure was calculated for each molecule, and the two structures were superimposed on the basis of the three conserved nucleotides ($A_8$, $A_9$, and $C_{10}$). The three nucleotides superimpose with an RMSD of less than 0.9 Å. Figure 9 shows how similar the two loops are and also where the common hydrogen bond is formed.

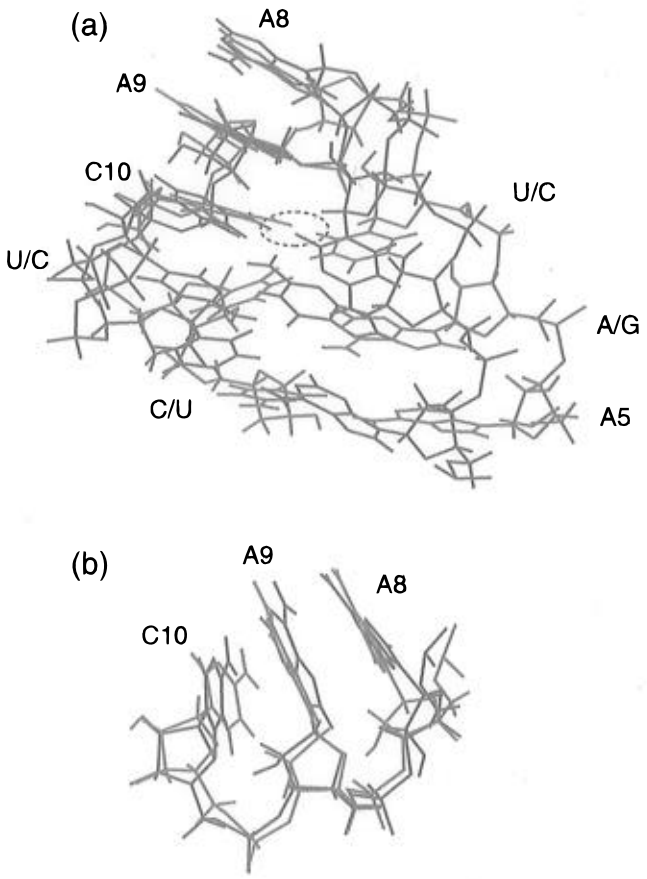


FIGURE 9: (a) Loop nucleotides of the superimposed average structures of the wild-type (in red) and the mutant (in blue) hairpins. In the case of the mutant hairpin, the formation of the two extra base pairs, $A_5$·$U_{12}$ and $G_6$·$C_{11}$, can be seen, while in the wild-type hairpin, the stacking of loop nucleotides $A_5$, $A_6$, $U_7$, and $C_{12}$ on the stem is visible. The hydrogen bond between the O2 of the seventh residue ($U_7$ in the wild-type and $C_7$ in the mutant) and the amino proton of $C_{10}$ is seen in both hairpins. The black circle indicates the position of this hydrogen bond. (b) Three conserved nucleotides, $A_8$, $A_9$, and $C_{10}$, from the overlapped average structures for the wild-type (red) and mutant (blue) hairpins shown from a slightly different view than in (a). The similarity in the structure is more clearly visible in this view.

The only significant difference between these two hairpins is the range over which the $^{31}$Ps resonate. In the case of the wild-type hairpin, they range over approximately 1 ppm, while in the mutant, this range is doubled to approximately 2 ppm. In both hairpins, the phosphorus of $A_8$ (i.e., of the 7p8 step) is the most downfield shifted. However, in the wild type it resonates at −3.29 ppm and is shifted by only ≈0.4 ppm from the rest of the stem $^{31}$P resonances, whereas in the mutant it resonates at −2.74 ppm and is shifted much more (≈1 ppm) from the nearest stem $^{31}$P resonance. Detailed analysis of each of the final structures for both the mutant and the wild-type hairpins shows that the $\alpha$ angle at this step has trans character in both hairpins. The average $A_8$ $\alpha$ angle for the wild-type hairpin is 141° (with a standard deviation of 15°) and that for the mutant is 169° (with a standard deviation of 6°). This indicates that, despite the differences in chemical shifts and the shift away from the stem, the conformation adopted by both loops in this region is quite similar. The detailed analysis of all the dihedral angles did, however, show other differences in the two structures. Apart from the trans $A_8$ $\alpha$, all other torsion angles in the mutant are very close to those expected in A-form RNA. However, in the case of the wild type, we see some

fluctuation from normal A-form RNA values, especially for the $\alpha$, $\gamma$, and, to a lesser extent, $\beta$ values of $U_{11}$. In both hairpins, some structures showed very different conformations about particular angles compared to the rest of the structures. The angles from such structures were not used in the calculation of the average. Such deviations, however, were few in number.

A minor difference between the structures of the two hairpins is evident from the superimposed ribbon representations of the phosphate backbones (Figure 7a of this and Figure 8a of the preceding paper). Unlike the mutant hairpin, some structures of the wild-type hairpin show a bend around nucleotide $U_{11}$. Also (see Figure 8b of the preceding paper), $U_{11}$ does not superimpose as precisely as the other nucleotides. We attribute this to having fewer NOE constraints for this region of the hairpin. The stem adopts a well-defined, A-form helix, residues $A_5$, $A_6$, $U_7$, and $C_{12}$ stack in A-form geometry on the stem, and long-range NOEs constrain the top of the loop. None of these constraints are available for the region near $U_{11}$, and hence, it is not as well defined. This is not the case in the mutant hairpin where the nucleotide in this position ($C_{11}$) is involved in the formation of a Watson−Crick base pair with $G_6$ and is very well constrained.

## DISCUSSION AND CONCLUSIONS

Selection experiments that were undertaken to determine what loop nucleotides were important for the sequence-specific binding of the mRNA to T4 DNA polymerase yielded the surprising answer that two loop sequences bind the polymerase with similar affinity (Tuerk & Gold, 1990). The two loops were different in that the mutant has two more base pairs in the stem and a smaller loop. Despite the difference, they bound the polymerase with equal affinity. This could be for a variety of reasons—the two hairpins could adopt similar three-dimensional structures, or it is possible that, upon binding to the polymerase, either the wild-type hairpin formed an $A^+$•C and A•U pair to make it similar to the mutant or the extra base pairs of the bound mutant were denatured. Yet another alternative is that these loops interact with other parts of the 36-nucleotide sequence (the minimum RNA sequence determined necessary for polymerase binding) and this is responsible for the correctly folded structure that the protein can recognize. In our study, we obtained the high-resolution structures of both hairpin molecules in order to explore the theory that the solution structures that these two hairpins present to the polymerase is similar. The results of our study indicate that this is indeed the case.

Our studies on the wild-type hairpin (see preceding paper) indicated that its stem was not confined to the four proposed base pairs. It is extended on both the 5′ and 3′ sides, and this results in the loop size being reduced to effectively only four nucleotides. Hydrogen bond interactions in the loop could help stabilize the loop and make it less flexible.

Despite differences in the sequence and proposed secondary structure, we find that the mutant hairpin adopts a three-dimensional conformation that is remarkably similar to that of the wild-type hairpin. The effective stem length and loop sizes are the same in both molecules. Despite a difference in the nucleotide (the wild type has a uracil at position 7 while the mutant has a cytosine), similar NOEs are noticed in the loop region to the sugar protons of this nucleotide. Similarly, the nucleotide at this (seventh) position is involved in the formation of a hydrogen bond with the $C_{10}$ amino proton. It is interesting that the substituted nucleotide is still capable of forming this hydrogen bond, and it is conceivable that this was the reason why this change was at all tolerated. Both hairpins show a turn in their backbones at the 7p8 step even though the seventh residue is not common and even though the loop is large enough to have tolerated the bend at any other position. This turn positions the three conserved loop nucleotides ($A_8$, $A_9$, and $C_{10}$) in perfect orientation so that their bases can project out into solution. We believe this is the key to the two structures. It is likely that the protein uses these three nucleotides, which are pointing out into solution in both molecules as a way of recognizing the mRNA. The conserved conformation of these three nucleotides explains how a different loop sequence binds the DNA polymerase as well as the wild-type hairpin does.

## ACKNOWLEDGMENT

We thank Ms. Barbara Dengler for managing the laboratory and Mr. David Koh for synthesizing the DNA templates. We are also grateful to Dr. Gabriele Varani for his critical reading of the manuscript.

## REFERENCES

Altona, C. (1982) *Recl. Trav. Chim. Pays-Bays 101*, 413−433.
Andrake, M., Guild, N., Tien, H., Gold, L., Tuerk, C., & Karam, J. (1988) *Proc. Natl. Acad. Sci. U.S.A. 85*, 7942−7946.
Brünger, A. T. (1990) *X-PLOR: A System for Crystallography and NMR, Version 2.1*, Yale University, New Haven, CT.
de Leeuw, F. A. A. M., & Altona, C. (1982) *J. Chem. Soc., Perkin Trans. 2*, 375−384.
Giessner-Prettre, C., Pullman, B., Ribas Prado, F., Cheng, D. M., Iuorno V., & Tso, P. O. P. (1984) *Biopolymers 23*, 377−388.
Gorenstein, D. G. (1984) *Phosphorus-31 NMR: Principles and Applications* (Gorenstein, D. G., Ed.) Academic Press, New York.
Heus, H. A., & Pardi, A. (1991) *J. Am. Chem. Soc. 113*, 4360−4361.
Milligan, J. F., Groebe, D. R., Witherell, G. W., & Uhlenbeck, O. C. (1987) *Nucleic Acids Res. 15*, 8783−8798.
Plateau, P., & Gueron, M. (1982) *J. Am. Chem. Soc. 104*, 7310−7311.
Puglisi, J. D., & Tinoco, I., Jr. (1989) *Methods Enzymol. 180*, 304−325.
Saenger, W. (1984) *Principles of Nucleic Acid Structure*, Springer-Verlag, New York.
Tuerk, C., & Gold, L. (1990) *Science 249*, 505−510.
Tuerk, C., Eddy, S., Parma, D., & Gold, L. (1990) *J. Mol. Biol. 213*, 749−761.
Varani, G., & Tinoco, I., Jr. (1991) *Q. Rev. Biophys. 24*, 479−532.
Varani, G., Cheong, C., & Tinoco, I., Jr. (1991) *Biochemistry 30*, 3280−3289.
Williamson, J. R., & Boxer, S. G. (1989) *Biochemistry 28*, 2819−2831.
Wyatt, J. R., Chastain, M., & Puglisi, J. D. (1991) *BioTechniques 11*, 764−769.

BI960415Q